Earthquake Engineering & Structural Dynamics
The Journal of the International Association for Earthquake Engineering

EARTHQUAKE ENGINEERING & STRUCTURAL DYNAMICS
Earthquake Engng Struct. Dyn. (2014)
Published online in Wiley Online Library (wileyonlinelibrary.com). DOI: 10.1002/eqe.2406

Dynamic response analysis of solitary flexible rocking bodies: modeling and behavior under pulse-like ground excitation

Michalis F. Vassiliou[1,*,†], Kevin R. Mackie[2] and Božidar Stojadinović[1]

[1]*Institute of Structural Engineering (IBK), Swiss Federal Institute of Technology (ETHZ), Stefano-Franscini-Platz 5, 8093, Zürich, Switzerland*
[2]*University of Central Florida, Civil Environmental and Construction Engineering Department, Orlando, FL 32816-2450, USA*

SUMMARY

Results obtained for rigid structures suggest that rocking can be used as seismic response modification strategy. However, actual structures are not rigid: structural elements where rocking is expected to occur are often slender and flexible. Modeling of the rocking motion and impact of flexible bodies is a challenging task. A non-linear elastic viscously damped zero-length spring rocking model, directly usable in conventional finite element software, is presented in this paper. The flexible rocking body is modeled using a conventional beam-column element with distributed masses. This model is verified by comparing its pulse excitation response to the corresponding analytical solution and validated by overturning analysis of rocking blocks subjected to a recorded ground motion excitation. The rigid rocking block model provides a good approximation of the seismic response of solitary flexible columns designed to uplift when excited by pulse-like ground motions. Guidance for development of rocking column models in ordinary finite element software is provided. Copyright © 2014 John Wiley & Sons, Ltd.

Received 19 May 2013; Revised 10 December 2013; Accepted 2 January 2014

KEY WORDS: rocking structures; fem modelling; overturning stability; seismic response

1. INTRODUCTION

Early studies of the response of rigid blocks allowed to uplift and rock under seismic motion have been presented by Milne [1]. Housner [2] has shown a scale effect that characterizes the response of rocking blocks subjected to a ground motion: a) for a given earthquake, larger objects need a larger ground acceleration to overturn, and b) longer dominant period earthquakes have a larger overturning capability than shorter dominant period ones. For pulse-like records, the above results were presented in the form of rocking spectra by Zhang and Makris [3] and Makris and Konstantinidis [4]. In the latter paper, the representation of a rigid rocking block as a single-degree-of-freedom (SDOF) linear-elastic system, which is a representation adopted by building codes (e.g. FEMA 356), is shown to be fundamentally flawed. Instead, rigid rocking blocks can be modeled as SDOF nonlinear-elastic viscously-damped systems. Ordinary finite element method (FEM) software equipped with nonlinear-elastic spring elements and with nonlinear geometry capabilities can model the rocking seismic response of both rigid and flexible bodies. This model extends the lumped plasticity models reviewed in [5] to account for the energy dissipated due to impact. It is simpler and computationally faster than the multi-spring models reviewed in [5]. Hence, this model can be used to study the influence of flexibility on the response of rocking structures, a phenomenon that has been examined by Psycharis [6],

*Correspondence to: Michalis F. Vassiliou, Institute of Structural Engineering (IBK), Swiss Federal Institute of Technology (ETHZ), Stefano-Franscini-Platz 5, 8093, Zürich, Switzerland.
†E-mail: mfvassiliou@gmail.com

Ichinose [7], Olivetto et al. [8], Spyrakos and Nikolettos [9], Apostolou et al. [10], and recently by Acikgoz and DeJong [11]. The interest in the influence of the flexibility of structures on their rocking behavior originates from the studies on the feasibility of using rocking as a seismic response modification technique characterized by small residual displacements and small forces transmitted to foundations (Housner [2], Meek [12], Chopra and Yim [13], Psycharis [14], Apostolou et al. [10], Gelagoti et al [15], Makris and Vassiliou [16]). A bridge that uses rocking in such manner has already been built in the Rangitikei River in New Zealand in 1981 (Beck and Skinner [17]). Moreover, it has been shown that ancient columns have survived earthquakes for more than 2,500 years due to their ability to sustain rocking motion without overturning (Konstantinidis and Makris [18]).

2. ROCKING RESPONSE OF A RIGID BLOCK

With reference to Figure 1 (top, center) and assuming that the coefficient of friction is large enough so that there is no sliding, the equation of motion of a free standing rigid block with size $R = \sqrt{h^2 + b^2}$ and slenderness $\alpha = \text{atan}(b/h)$ subjected to a horizontal ground acceleration $\ddot{u}_g(t)$, when rocking around O and O′ respectively is (Yim et al. [19], Makris and Roussos [20], Zhang and Makris [3], among others):

$$I_o\,\ddot{\theta}(t) + mgR\sin[\alpha\,\text{sgn}\theta(t) - \theta(t)] = -m\,\ddot{u}_g(t)R\cos[\alpha\,\text{sgn}\theta(t) - \theta(t)] \tag{1}$$

For initiation of the rocking motion, $\ddot{u}_g(t) > g\tan\alpha$ must occur during the excitation. The corresponding acceleration needed to trigger sliding is μg, which is larger than the acceleration to trigger rocking for common interface materials and slenderness ratios.

For rectangular blocks $I_o = (4/3)mR^2$, and the above equations can be expressed in a compact form as:

$$\ddot{\theta}(t) = -p^2\left\{\sin[\alpha\,\text{sgn}(\theta(t)) - \theta(t)] + \frac{\ddot{u}_g}{g}\cos[\alpha\,\text{sgn}(\theta(t)) - \theta(t)]\right\} \tag{2}$$

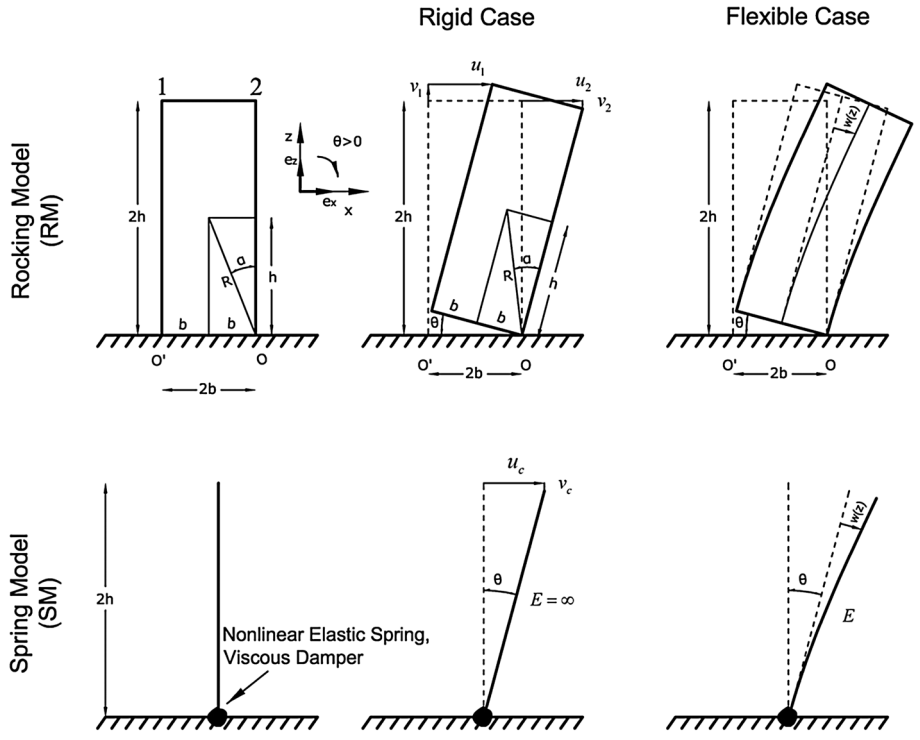

Figure 1. Rocking Model (top) and the proposed Spring Model (bottom).

DOI: 10.1002/eqe

The oscillation frequency of a rigid block under free vibration is not constant because it strongly depends on the vibration amplitude (Housner [2]). Nevertheless, the quantity $p = \sqrt{\frac{3g}{4R}}$ is a measure of the dynamic characteristics of the block and is equal to the in-plane pendulum frequency of the block as if it were hanging from its rocking rotation point (Dimitrakopoulos and DeJong [21]). For the 7.5m × 1.8m free-standing column of the Temple of Apollo in Corinth p =1.4 rad/s.

Figure 2 (left) shows the moment-rotation relationship during the rocking motion of a free-standing rigid block. The system has infinite stiffness until the magnitude of the applied moment reaches the value $mgR\sin\alpha$. Once the block is rocking, its restoring force decreases monotonically, reaching zero when $\theta = \alpha$. This negative stiffness, inherent to rocking systems, is attractive because it keeps the base shear and moment transmitted to the foundation bounded (Makris and Konstantinidis [4]), provided that the rocking block remains stable. During the oscillatory rocking motion, the moment-rotation response follows the curve shown in Figure 2 (right) without enclosing any area. Energy is lost only during impact, when the angle of rotation reverses. Conservation of angular momentum an instant before the impact and immediately after the impact gives the coefficient of restitution:

$$r = \frac{\dot{\theta}_2^2}{\dot{\theta}_1^2} = \left[1 - \frac{3}{2}\sin^2\alpha\right]^2 \tag{3}$$

3. NONLINEAR ELASTIC VISCOUSLY DAMPED SPRING MODEL

Equations (2) and (3) can be easily solved using a numerical computing package (e.g., MATLAB [22]). This numerical solution is denoted the Rocking Model (RM) throughout. However, the equations of more complex rocking structures or flexible rocking structures become much more complicated and their solution becomes cumbersome. Therefore, an equivalent nonlinear-elastic viscously-damped Spring Model (SM) that does not involve explicit modeling of rocking body impact is proposed (Figure 1, bottom).

The proposed model consists of a cantilever linear elastic column, with cross section identical to the cross section of the rocking block, connected to a nonlinear-elastic rotation spring. This spring has a rigid-plastic moment-rotation response envelope with a yield moment equal to $mgRsin(\alpha)$ and unloads along the loading path, as shown in Figure 2, right. Second-order geometric transformations and large displacements are taken into account in the SM to capture the negative stiffness of the RM, shown in Figure 2 (left). A viscous damper with damping coefficient c is added in parallel with the nonlinear elastic spring in the SM. When the response of the SM is compared to that of the RM in this paper, the Young's modulus, E, of the SM column material is set to a very large value such that the column is quasi-rigid.

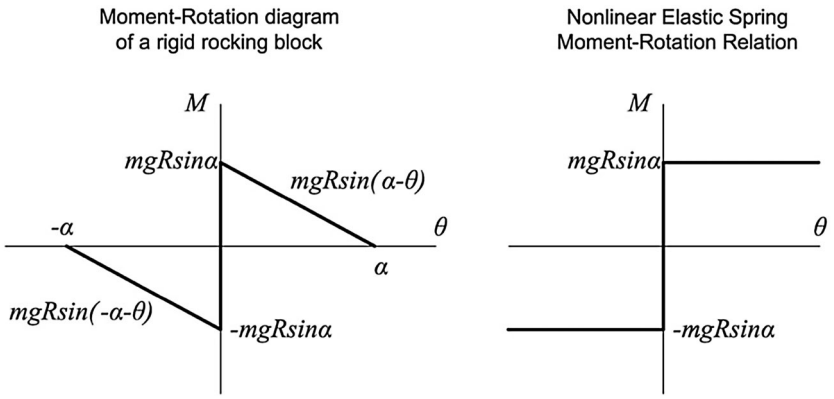

Figure 2. Moment rotation relationships for a rigid rocking block with slenderness α and size R (left) and a nonlinear elastic spring of the proposed SM (right).

DOI: 10.1002/eqe

Modeling the rigid rocking body using kinematic constraints, e.g., constraining the relative horizontal motion of the nodes of the column in the SM, was purposely avoided. Such constraints are typically implemented using first-order geometry and small displacement assumption, and thus typically result in inadvertent introduction of forces in the rigid body during rocking response simulations. The proposed SM was implemented in the FEM software framework OpenSees [23] and can be easily implemented in commercial FEM software. The rocking body was modeled as a flexible beam using elastic displacement formulated beam-column elements.

3.1. Comparison of the displacements

The rotation-horizontal displacement relations of the RM are (Figure 1, top-center):

$$u_1 = \begin{cases} 2R\cos\alpha\sin\theta, & \theta < 0 \\ 2R(\sin\alpha - \sin(\alpha-\theta)), & \theta > 0 \end{cases}$$
$$u_2 = \begin{cases} 2R(\sin\alpha - \sin(\alpha+\theta)), & \theta < 0 \\ 2R\cos\alpha\sin\theta, & \theta > 0 \end{cases} \tag{4}$$

The rotation-horizontal displacement of the SM (Figure 1, bottom-center) is:

$$u_c = 2R\cos\alpha\sin\theta. \tag{5}$$

Similarly, the vertical displacements of the RM are:

$$v_1 = \begin{cases} -2R\cos\alpha(1-\cos\theta), & \theta < 0 \\ 2R(\cos(\alpha-\theta) - \cos\alpha), & \theta > 0 \end{cases}$$
$$v_2 = \begin{cases} 2R(\cos(\alpha+\theta) - \cos\alpha), & \theta < 0 \\ -2R\cos\alpha(1-\cos\theta), & \theta > 0 \end{cases} \tag{6}$$

while, those of the SM is:

$$v_c = -2R\cos\alpha(1-\cos\theta) \tag{7}$$

Similar equations exist for the displacement of the middle point of the top cross section.

The above displacements, normalized by the size of the rocking block $2R$, are plotted in Figure 3 for the RM and SM for two different values of slenderness α. Figure 3 shows that the horizontal displacements of the two models agree well for both cases. Though the vertical displacements do not match, it will be shown later that this drawback does not jeopardize the model's ability to accurately capture the rotation and horizontal displacement of a solitary column due to ground excitation. This behavior may impede the use of the SM to model post-tensioned rocking blocks (Barthes et al. [24]).

3.2. Comparison of the pushover curves

The horizontal force-displacement pushover response curve for the RM (with the force acting at the centroid of the rocking block) is given by

$$\frac{F}{mg} = \tan(\alpha-\theta) \tag{8}$$

while the pushover curve for the SM (with the force acting at the middle of the column) is given by

DOI: 10.1002/eqe

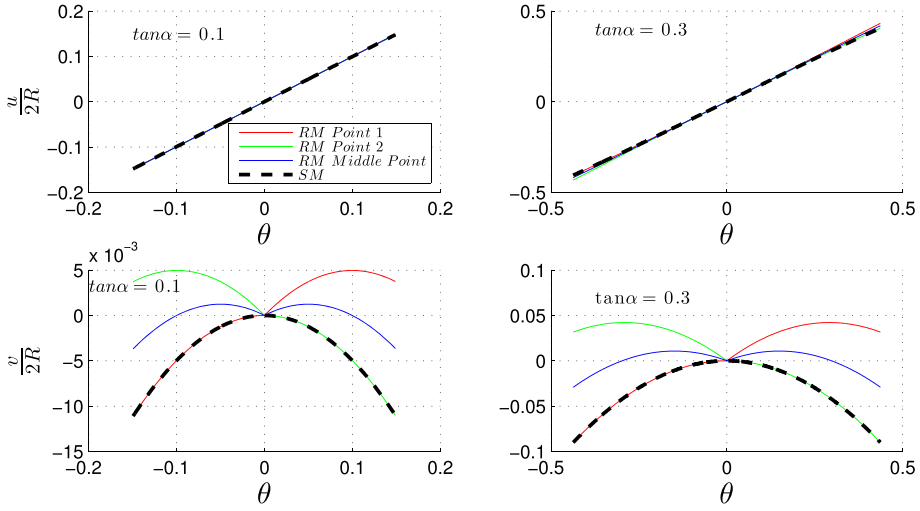

Figure 3. Comparison of the horizontal (top) and vertical (bottom) displacements of the RM and the SM for two different values of slenderness α.

$$\frac{F}{mg} = \left(\frac{\tan\alpha}{\cos\theta} - \tan\theta\right) \tag{9}$$

The two pushover curves are shown in Figure 4 for two slenderness values: the two models agree well.

3.3. *Comparison of the equations of motion*

The equation of motion of the SM (disregarding damping) is

$$I_o^{'}\,\ddot{\theta}(t) + mgR(\sin\alpha\,\mathrm{sgn}\theta - \cos\alpha\sin\theta) = -m\,\ddot{u}_g R\cos\alpha\cos\theta \tag{10}$$

where

$$I_o^{'} = \frac{4}{3}mR^2\cos^2\alpha \tag{11}$$

For small θ and α and retaining only the linear terms, the equation of motion of the RM (1) reduces to

$$I_o\,\ddot{\theta}(t) + mgR(\alpha\,\mathrm{sgn}\theta - \theta) = -m\ddot{u}_g R \tag{12}$$

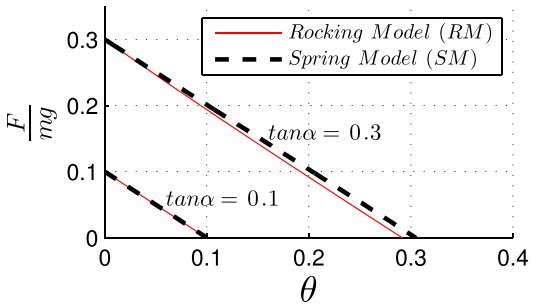

Figure 4. Force-deformation pushover curves for the RM and the SM.

DOI: 10.1002/eqe

Linearizing equation (10) gives equation (12), too. Hence, linearization of the equations of motion for both models leads to the same result (i.e., differences between the two models arise only from the nonlinear terms).

The responses of rigid ($E = 10^{11}$kPa) 10m tall blocks with slenderness ratio values $\tan\alpha = 0.1$, 0.2 and 0.3 to a symmetric Ricker pulse [25] excitation with $a_p = 4g\tan\alpha$ and $\omega_p = 2\pi$ rad/s (Figure 5 – bottom) are computed next using the RM (Equation (1)) and the SM implemented in OpenSees. Assuming zero damping for both models (i.e., $c = 0$ and $r = 1$), the rotation time histories are plotted in Figure 5 (left). For $\tan\alpha = 0.1$, the two models agree very well. However, for larger α (i.e., more squat objects) the match is not as close. Since the pushover curves (Figure 4) match well even for $\tan\alpha = 0.3$, it is reasonable to assume that this error comes from the difference in the moments of rotational inertia of the two models. Namely, the rotational inertia in the RM refers to rotation about the corner of the rigid block ($I_o = \frac{4}{3}mR^2$), while the rotational inertia in the SM refers to the mid-point of the rigid block base ($I_o^{'} = \frac{4}{3}mR^2\cos^2\alpha$) and does not account for the shape of the rocking body. For very slender structures (e.g., $\tan\alpha = 0.1$) the addition of the rotational mass makes the results slightly worse. This might be attributable to when other sources of error (simplifications made in equation (12)) become dominant. Nevertheless, for $\tan\alpha = 0.1$ the results obtained from models with and without extra masses match the RM results pretty well. On the other hand, for less slender structures Figure 5 (middle and bottom) shows that the model with the extra masses behaves much better.

For this reason, the SM was modified by evenly distributing the rotational inertia difference $\Delta I_o = {}^4/_3 mR^2(1 - \cos^2 a)$ among the rotational degrees of freedom of the nodes used to model the column. Namely, a rotational mass equal to $\frac{\Delta I_o}{nnod}$ (where *nnod* is the number of nodes) is added to the rotational degree of freedom of each node in the finite element model. Adding rotational inertia to the column in the SM becomes more important as the rotational inertia of the cross-section of the rocking body

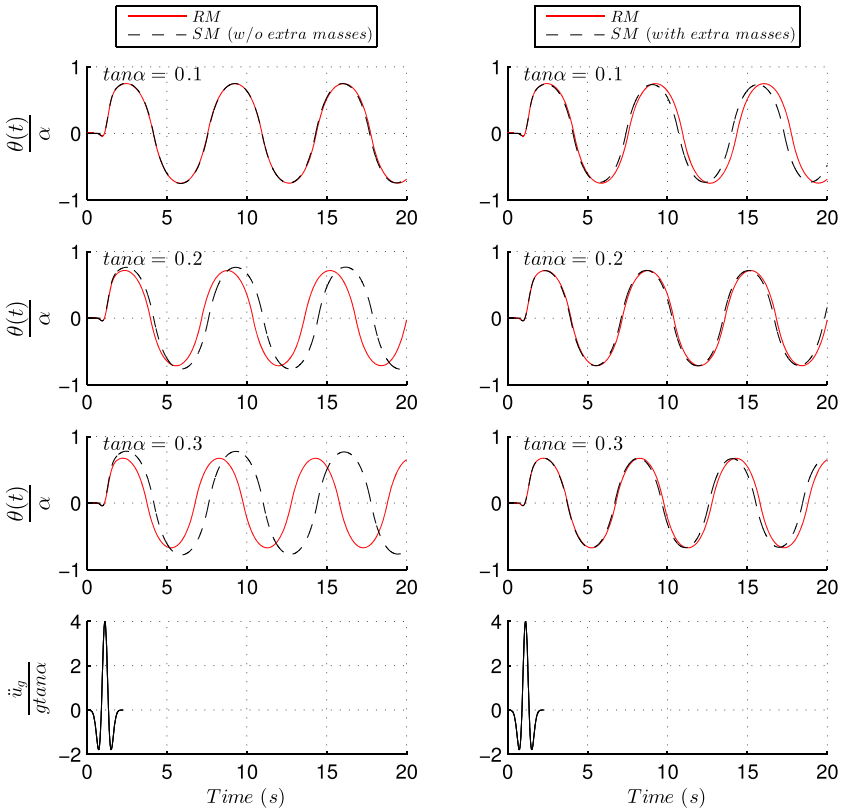

Figure 5. Rocking rotation time history response of undamped rigid blocks to a symmetric Ricker pulse excitation (bottom row). The plots compare the RM to the SM with (right column) and without (left column) added rotational nodal masses.

DOI: 10.1002/eqe

increases and as the rocking block becomes less slender. The rotation time histories for the SM with added rotational masses are plotted in Figure 5 (right).

The overturning spectra (contours of normalized maximum rotation θ/α) for a rigid rocking block excited by a symmetric Ricker pulse [25] of amplitude a_p and cyclic frequency ω_p computed using the RM and the SM without and with the distributed rotational masses are plotted in Figure 6. The ordinate of the spectra plots shows the excitation intensity in terms of peak pulse acceleration normalized by the gravity acceleration and the aspect ratio of the rocking block. The abscissa of the spectra shows the dominant frequency of the excitation pulse normalized by the frequency parameter p of the rocking block. Small values on the abscissa represent small rocking blocks and long pulse excitation dominant period values, while large abscissa values represent large rocking blocks and short pulse excitation dominant period values. The spectra show good agreement of the three models.

Numerical issues arise when the pre-yielding stiffness of the nonlinear elastic spring is very large, representing rigid bodies rocking on a rigid foundation. Hence, time-adaptive numerical integration schemes were used to allow for a small time step to be taken when the rocking block is in full contact with the foundation, and for a large time step to be used during the rotation of the block about either edge. These numerical issues vanish if the flexibility of the ground on which the column rocks is accounted for by using a softer pre-yielding branch of the nonlinear elastic spring moment-rotation backbone curve [26].

3.4. *Treatment of energy dissipation*

Energy dissipation in rocking blocks takes place instantaneously at each impact. For the RM, the energy dissipation ratio (E/E_o) per cycle of free rocking (initial conditions $\theta(0) = \theta_o$ and $\dot{\theta}(0) = 0$) is independent of the amplitude of rocking and is described by the restitution factor r. The ratio of the energy at the end of one complete cycle, E, to the energy at the beginning of that cycle, E_o, is

$$\frac{E}{E_o} = r^2 = \left(1 - \frac{3}{2}\sin^2\alpha\right)^4 \tag{13}$$

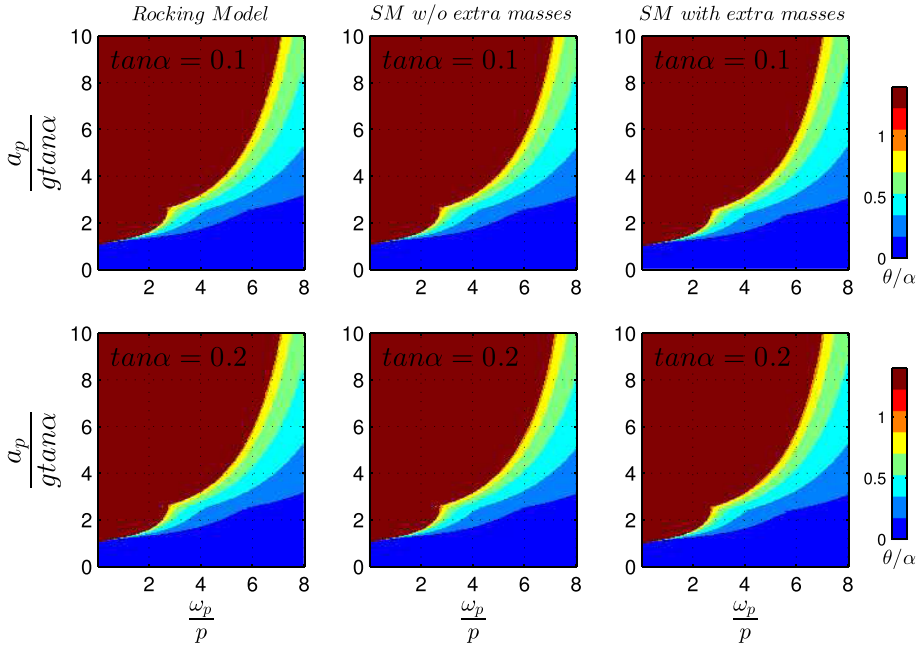

Figure 6. Contour plots of the normalized maximum rotation, θ/α, of undamped rigid blocks subjected to a symmetric Ricker pulse: RM (left column), SM without the nodal rotational masses (middle column), and SM with the nodal rotational masses (right column).

DOI: 10.1002/eqe

On the other hand, viscous damping models widely used in structural dynamics, dissipate energy continuously in proportion to an associated relative velocity. Despite this fundamental difference, the proposed SM utilizes a viscous damper with a damping coefficient c associated with the column rotation velocity located at the base of the column. This is intended to account only for energy dissipated during impacts of the rigid body, and does not account for any additional engineered dampers (e.g., Mariott et al. [27]). It is further assumed, without verification, that the energy dissipated through rocking impact does not depend strongly on the flexibility of the rocking body, and thus, on the flexibility of the column in the SM.

The damping in the SM is also different from the Rayleigh damping model used by Wiebe et al. [28] in that it is based on equivalent viscous damping corresponding to energy dissipation in a single cycle.

The equivalent per-cycle energy loss ratio, r_{eq}^2, for the SM is a function of 6 variables:

$$\frac{E}{E_o} = r_{eq}^2 = f(m, \alpha, R, g, \theta_o, c) \tag{14}$$

Each term of equation (14) includes only 3 reference dimensions (r_{eq}^2 =[], α = [], R = [L], g = [LT^{-2}], θ_o = [], c = [ML^{2}T^{-1}]). Hence, according to Buckingham's Π theorem of dimensional analysis [29], equation (14) can be transformed into

$$\frac{E}{E_o} = r_{eq}^2 = \varphi\left(\frac{\theta_o}{\alpha}, \alpha, \overline{c}\right) \tag{15}$$

where $\overline{c} = \frac{c}{mg^{0.5}R^{1.5}}$. If the SM were hanging from its rotation point, its small amplitude rotation vibration damping ratio would be equal to $\left(2\sqrt{\frac{1}{3} + \cos^2\alpha}\right)^{-1}\overline{c}$.

Equation (15) is plotted in Figure 7 for $0 < \theta_o/\alpha < 1$, tanα equal to 0.1, 0.2 and 0.3, and $\overline{c}$ equal to 0.02, 0.08 and 0.18. The plot shows that: a) for constant θ_o/α and $\overline{c}$, r_{eq}, (which is a measure of damping in the SM) the response of the SM (not of the actual rocking body) does not depend on α; and b) that for $\theta_o/\alpha > 0.5$, r_{eq} depends on θ/α only slightly. Hence for $\theta/\alpha > 0.5$ and tanα <0.3, equation (16) reduces to

$$\frac{E}{E_o} = r_{eq}^2 = \varphi(\overline{c}) \tag{16}$$

Equations (13) through (16) indicate that a relation between $\overline{c}$ and α can be determined such that the energy losses during a free rocking cycle in the RM and the SM are the same (for $\theta_o/\alpha > 0.5$, fairly large rocking angles). Based on the data in Figure 7, the following relationship for $\theta_o/\alpha > 0.5$ is proposed:

$$\overline{c} = \frac{c}{mg^{0.5}R^{1.5}} = 0.02\left(\frac{\alpha}{0.1}\right)^2 \tag{17}$$

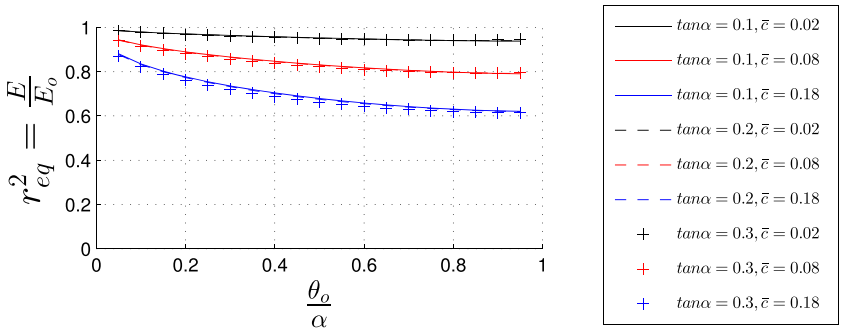

Figure 7. Damping ratio, r_{eq}^2, plotted against the normalized initial angle of rotation θ_o/α for free vibrations of the SM (with extra masses) for three different values of parameters α and $\overline{c} = \frac{c}{mg^{0.5}R^{1.5}}$.

DOI: 10.1002/eqe

Equation (17) makes it possible to define the per-cycle equivalent energy loss damping coefficient for the rotational damper in the SM as a function of the body mass, size and slenderness:

$$c = 0.02\left(\frac{\alpha}{0.1}\right)^2 mg^{0.5}R^{1.5} \tag{18}$$

ElGawady et al. [30] have shown that the energy dissipated in a rocking body impact depends not only on slenderness, α, but also strongly on the interface material on the rocking surfaces. Therefore, further research is needed to account for the type of interface material in the equivalent viscous damper of the SM. Moreover, note that since the damping coefficient was calibrated for large angles of rotation, the following analysis is suitable for overturning analysis of blocks and not for small angle uplift.

The time histories of the rocking response of a 10m tall block with slenderness ratio values $\tan\alpha = 0.1$, 0.2 and 0.3 to a symmetric Ricker [25] pulse excitation computed using the RM and the SM (with damping) are plotted in Figure 8. In all cases, the proposed SM is able to accurately predict the maximum rotation of the base of the rocking body. For the most slender case ($\tan\alpha = 0.1$) the SM is able to accurately predict the entire time history. The SM is not as good in the least slender case ($\tan\alpha = 0.3$) because of the highly nonlinear nature of the rocking problem. Namely, the period of free rocking depends on the amplitude of the motion. Hence a small error in the estimate of the amplitude leads to error in the prediction of the phase of the motion.

The overturning spectra for the two models are plotted in Figure 9 to show that the SM with added rotational masses matches the results obtained using the RM very well. Figure 10 plots the minimum overturning acceleration spectra for the El Centro ground motion, which is an as-recorded, non-pulse-like ground motion. The plot shows that the proposed SM matches the results of the RM well for slenderness $\alpha < 0.3$. It should be noted that this is a case-specific example of the expected error and

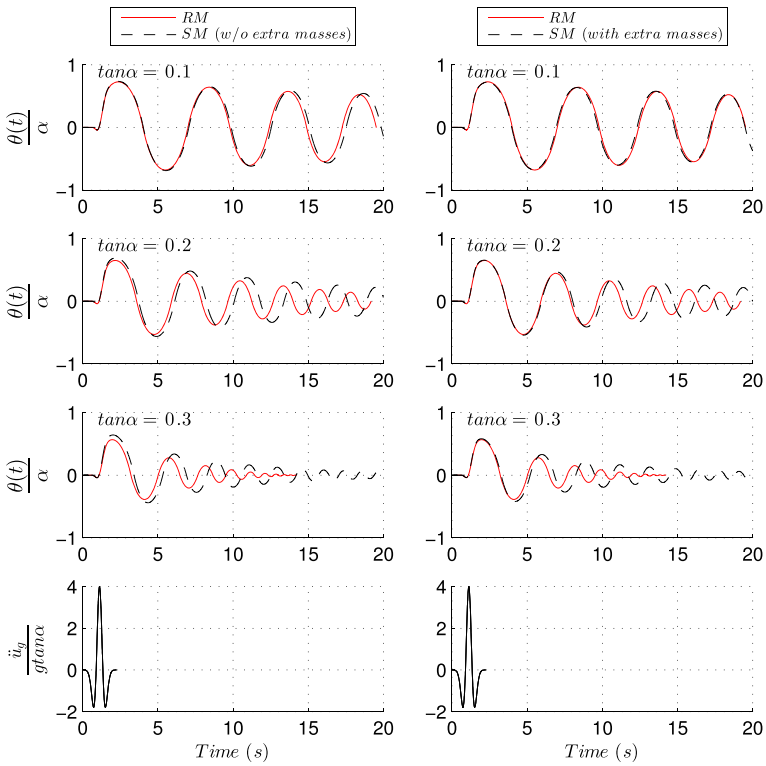

Figure 8. Time history response of a damped rigid block with height 10m and slenderness $\tan\alpha = 0.1$, 0.2 and 0.3 (top 3 rows) excited by a symmetric Ricker pulse excitation with $a_p = 4g\tan\alpha$ and $\omega_p = 2\pi$ rad/s (bottom row). The response was computed with the RM, the SM with (right column) and without (left column) the added rotational masses.

DOI: 10.1002/eqe

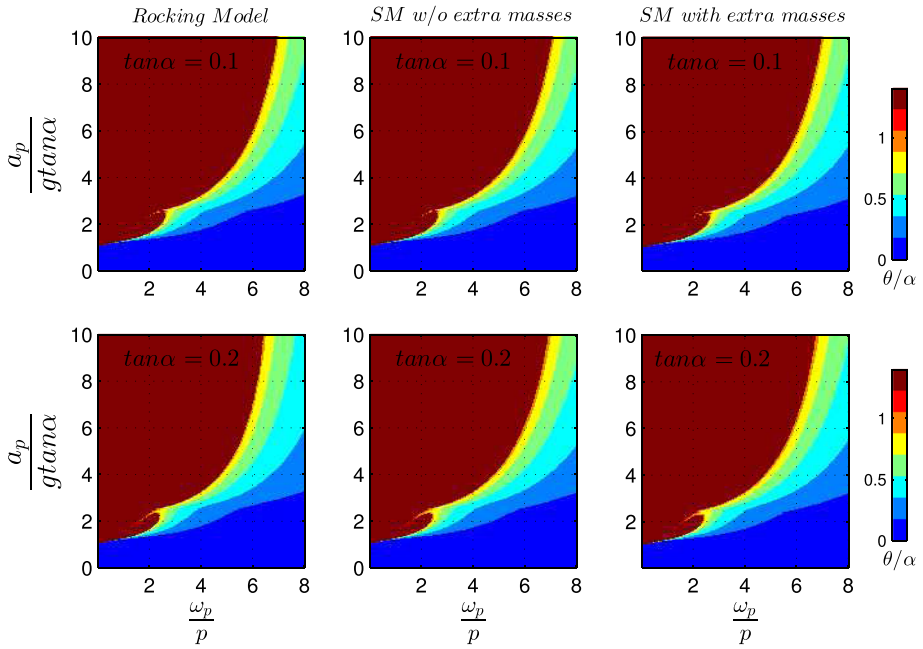

Figure 9. Contour plots of the normalized maximum rotation, θ/α, of damped rigid blocks subjected to a symmetric Ricker pulse: RM (left column), SM without the nodal rotational masses (middle column), and SM with the nodal rotational masses (right column).

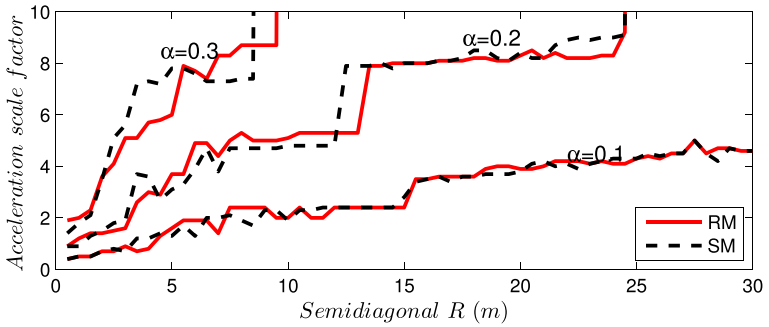

Figure 10. Minimum overturning acceleration spectrum for the El Centro ground motion. The El Centro ground motion is scaled up until the block overturns. The ordinate of the plot shows the scaling factor.

that there is no definite trend on whether the SM overestimates or underestimates the response when compared with RM.

4. EXTENSION TO FLEXIBLE SYSTEMS

Even though rocking of rigid structures has been studied extensively, relatively few studies have been carried out to investigate the influence of the flexibility of a structure on its rocking behavior [11, 13]. An investigation of rocking of flexible blocks and an examination of the limits of the validity of the rigid block assumption is presented in this section. The SM with damping enhanced by additional rotational masses was extended by assuming that the column, which represents the rocking body, is deformable. It is modeled as an Euler-Bernoulli beam-column with a linear elastic material characterized by the elastic modulus E and density ρ. This model is shown in Figure 1, right.

DOI: 10.1002/eqe

Roh and Reinhorn [31] performed experiments on rocking concrete columns and proved that, for low values of axial force, spalling of concrete does not occur when the column uplifts. Therefore, it is assumed that the geometry of the rocking interface does not change and that the column will rotate around points O and O′. Furthermore, since the vertical reaction at the rocking point (equal to the self-weight of the rocking body) is relatively small, the compression zone of the base cross section tends to become a point.

4.1. Dimensional analysis of flexible rocking systems

The overturning instability of a flexible rocking column subjected to a symmetric Ricker pulse is described by its base rotation and is a function of 7 variables.

$$\theta(t) = f\left(a_p, \omega_p, g, R, \alpha, \zeta, \rho, E\right) \tag{19}$$

Each term of equation (19) includes only 3 reference dimensions ($a_p = [\mathrm{LT}^{-2}]$, $\omega_p = [\mathrm{T}^{-1}]$, $g = [\mathrm{LT}^{-2}]$, $R = [\mathrm{L}]$, $\alpha = []$, $\zeta = []$, $\rho = [\mathrm{ML}^{-3}]$, $E = [\mathrm{ML}^{-1\text{-}2}]$). The damping ratio, ζ, is the column first mode flexural vibration damping ratio, modeled in OpenSees using stiffness proportional Rayleigh damping for the nodes of the column, excluding the nodes at the end of the nonlinear spring (an option available in OpenSees). Energy dissipation due to rocking is modeled using the calibrated viscous damper of the SM. Hence, according to Buckingham's Π theorem of dimensional analysis [29], equation (19) can be transformed into

$$\theta(t) = \varphi\left(\frac{a_p}{g\tan\alpha}, \frac{\omega_p}{p}, \alpha, \zeta, \frac{E}{\rho g R}\right) \tag{20}$$

where $p = \sqrt{\frac{3g}{4R}}$.

The departure from the rigid case becomes significant when either $E/\rho g$ becomes small or when the column has a large size R. For a given material and slenderness α, the first eigenperiod of elastic vibration of the flexible solid rectangular column (without rocking) depends only on its size:

$$T_1 = 12.38\sqrt{\frac{\rho}{E}}\frac{h}{\tan\alpha} \tag{21}$$

The overturning spectra (contours of normalized maximum rotation θ/α) excited by a symmetric Ricker pulse [25] of amplitude a_p and cyclic frequency ω_p computed using the SM with the added rotational masses are plotted in Figure 11 for a quasi-rigid body and four different flexible rocking column heights with two different slenderness ratios. The flexible rocking bodies are assumed to be made of concrete ($E = 30GPa$ and $\rho = 2.5\mathrm{M}g/m^3$). The damping ratio, ζ, of the cantilever column was set to 0.01 assuming that the flexible rocking body remains elastic. The bold lines, defining the uplift initiation, rocking and overturning regions in the spectra plotted in Figure 11, are re-plotted in Figure 12. These plots show that for columns with $\tan\alpha > 0.2$, the flexibility of the column is immaterial to the overturning stability, and the rigid body approximation (RM) gives sufficiently accurate results.

For smaller values of $\tan\alpha$, Figure 12 indicates that the flexibility of the rocking body decreases the acceleration needed to cause uplift to values less than $g\tan\alpha$. This is because, for the range of ω_p/p plotted, the eigenperiods of the concrete column fall in the spectral region where the spectral acceleration is larger than the peak ground acceleration. The data in Figure 12 also shows that for $\omega_p/p < 4.5$ the flexible body is less stable than the rigid one (its overturning acceleration is smaller), while for $\omega_p/p > 4.5$ the flexible body exhibits superior stability. Therefore, the flexibility of rocking bodies has a negative influence on the stability of their rocking response only for the case in which large bodies (taller than 50m) experience pulses that give unrealistically small values of ω_p/p (i.e. corresponding to pulses with unrealistically long periods). Hence, for realistic values of ω_p/p and size, the flexibility of a rocking body makes it more stable under symmetric pulse excitations. Therefore, the analysis of the rocking response of concrete solitary columns of solid rectangular cross section to a

DOI: 10.1002/eqe

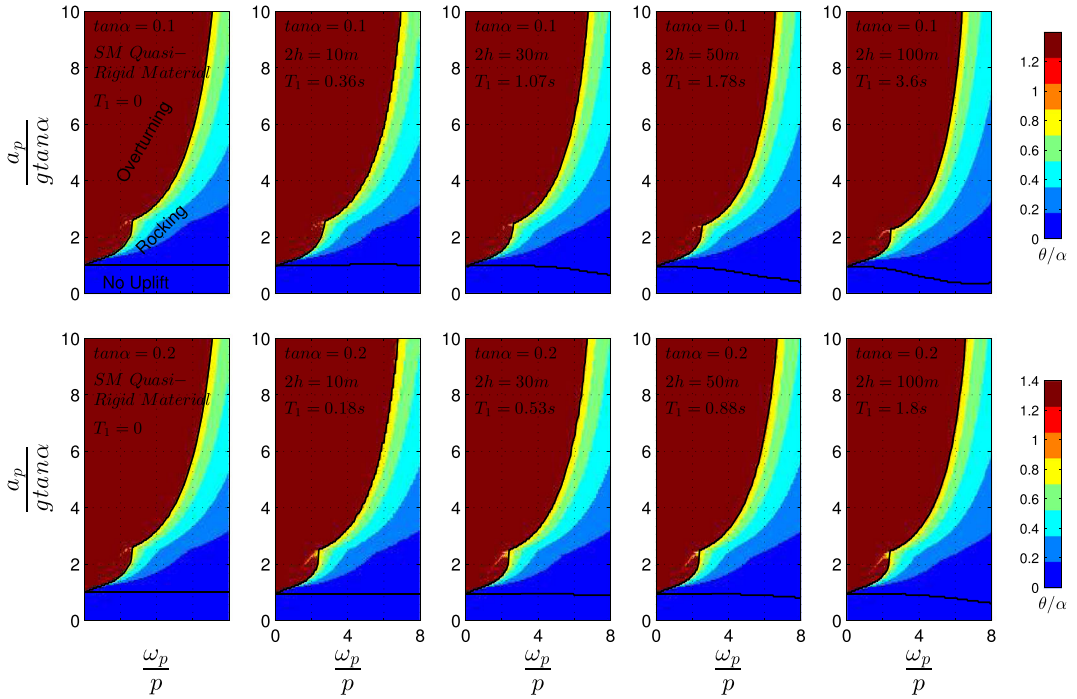

Figure 11. Contour plots of the normalized maximum rotation, θ/α, of quasi-rigid and concrete columns with height 2h and slenderness α when subjected to a symmetric Ricker acceleration pulse with amplitude a_p and cyclic frequency ω_p. The bold lines define the border between uplift and rocking regions as well as the minimum acceleration to cause overturning.

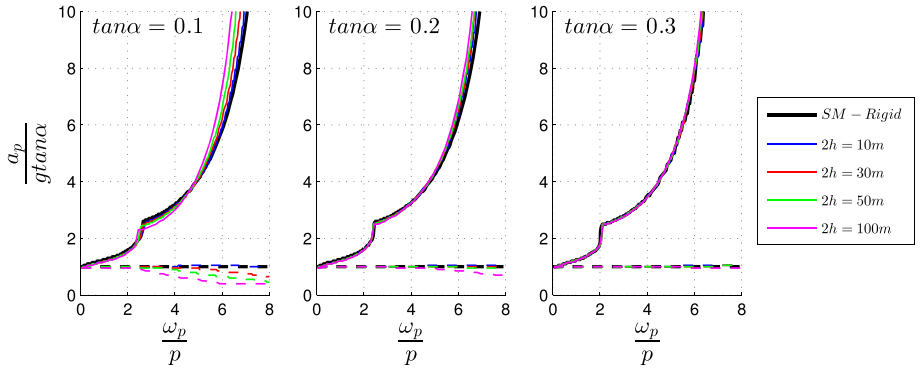

Figure 12. Comparison of the uplift and overturning acceleration spectra for quasi-rigid and flexible rocking bodies with height 2h and slenderness α when subjected to a symmetric Ricker acceleration pulse with amplitude a_p and cyclic frequency ω_p.

symmetric pulse excitation can be performed using a RM because it is either accurate enough (for small-size bodies) or on the conservative side (for larger size bodies). The effect of flexibility is even less significant for steel solid rectangular bodies since the ratio E/ρ is larger for steel than for concrete.

The interaction between flexibility and rocking for solid bodies is investigated next, paralleling the investigation for concentrated-mass single-degree-of-freedom systems presented by Chopra and Yim [13]. The responses of a rigid and a flexible (concrete material) rocking body with dimensions $2h = 50m$ and $2b = 5m$ excited by two different symmetric Ricker pulses, one with normalized frequency $\omega_p/p = 3$ ($T_p = 3.87$s) and normalized acceleration amplitude $a_p/g\tan\alpha = 2.6$ ($a_p = 2.55$m/s^2), the other with $\omega_p/p = 6$ ($T_p = 1.93$s) and $a_p/g\tan\alpha = 5.85$ ($a_p = 5.74$m/s^2), are computed and plotted in Figure 13. The first row plots the normalized rotation at the base of the column, θ/α, the second row plots the displacement

DOI: 10.1002/eqe

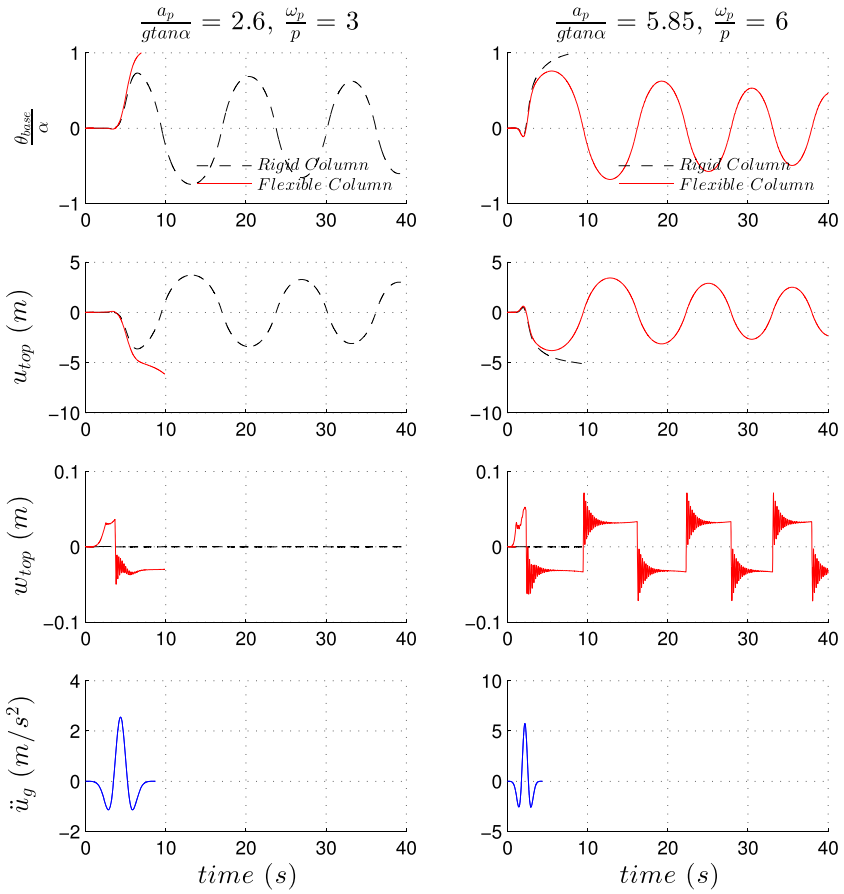

Figure 13. Comparison of time history response of a rigid and a flexible rocking column of slenderness α and frequency parameter p to a symmetric Ricker pulse with amplitude a_p and cyclic frequency ω_p. First row: normalized base rotation; second row: top displacement; third row: top displacement due to bending; forth row: ground acceleration

at the top of the column, u, and the third row plots the deformation at the top of the column, $w = u\text{-}2h\sin(\theta)$, i.e., the difference between the total top displacement and the top displacement due to base rotation (Figure 1 – right). The plots indicate that at each rocking impact, the deformation at the top caused by flexure reverses directions. This reversal generates flexural vibration in the column. Hence, part of the rotational kinetic energy of the flexible rocking body is transformed into high frequency flexural vibration energy, which cannot cause the rocking body to overturn. This transformation is the reason why the flexible rocking body is stable while the rigid rocking body overturns for $\omega_p/p = 6$. On the contrary, the longer pulse ($\omega_p/p = 3$) has smaller amplitude such that the first part of this pulse only slightly uplifts the rocking body. Then, the flexural vibration caused by the rocking impact is less intense, and most of the rotational kinetic energy is conserved, causing the flexible rocking body to overturn and the rigid rocking body to continue rocking.

Note that the flexible rocking body vibrates in flexure at a higher frequency than the fundamental fixed-base frequency of the same body. Moreover the flexural oscillations are damped out much faster than the $\zeta = 0.01$ damping ratio would indicate This behavior is in accordance with the findings of Chopra and Yim [13] and Acikgoz and DeJong [11] for a SDOF oscillator able to uplift.

5. ROCKING OF FLEXIBLE COLUMNS ON AN EXTENDED RIGID BASE

It is common to design columns in lateral force resisting fame systems as fully fixed to transmit the plastic-capacity column forces to the foundations. In turn, the foundations are designed to transmit

DOI: 10.1002/eqe

these forces to the underlying soil without uplift or soil failure. For most soil types, this requires extending the foundation substantially beyond the column section footprint and, sometimes, anchoring the foundation into the soil using piles. It has been proposed [15, 32–34] that the foundation of single columns could be allowed to rock in order to reduce the magnitude of the seismic forces in the structure and the foundations, and thereby control their size and cost. While this approach is effective, permanent soil deformations should be avoided as they may induce undesirable post-earthquake residual displacements of the foundations and the structure. Makris and Vassiliou [16] have shown that frames consisting of unconnected assemblies of rigid bodies rocking on an undeformable surface experience remarkable stability and suggested that uplift and rocking can be used as seismic response modification strategy. Then, the lateral forces used to design the rocking structure are controlled by the aspect ratio, the size of the rocking body and the stiffness of the foundation. However, the fluctuations of the top deflection shown in Figure 13 (3rd row) suggest that the design base moment is larger than the uplifting moment.

This concept is applied to a sole flexible rocking column (e.g., a tall chimney) fixed to an extended rigid foundation on undeformable soil, shown in Figure 14. First, the equation of motion of a rigid column with an extended rigid foundation is

$$\ddot{\theta}(t) = -p^{'2}\left\{ \sin\left[\alpha^{'} \operatorname{sgn}(\theta(t)) - \theta(t)\right] + \frac{\ddot{u}_g}{g} \cos\left[\alpha^{'} \operatorname{sgn}(\theta(t)) - \theta(t)\right] \right\} \tag{22}$$

where

$$p^{'2} = \frac{mgR^{'}}{I_o^{'}} \tag{23}$$

and $I_o^{'}$ is the moment of inertia of the rocking system around the pivot point equal to

$$I_o^{'} = \frac{1}{3}mR^2 + mR^2 \frac{\cos\alpha}{\cos\alpha^{'}} \tag{24}$$

Equations (23) and (24) give

$$p^{'2} = p^2 \frac{4\cos\alpha}{3\cos\alpha + \cos\alpha^{'}}, \tag{25}$$

resulting in $p \approx p'$ for small α and α'. The column uplift acceleration is

$$\ddot{u}_g^{uplift} = g\tan\alpha^{'} \tag{26}$$

and the restitution factor is

$$r^{'} = \left(1 - \frac{3}{2}\sin^2 a^{'} \frac{\cos^2\alpha}{\cos\alpha^{'}} \frac{4}{\cos\alpha^{'} + 3\cos\alpha}\right)^2 \tag{27}$$

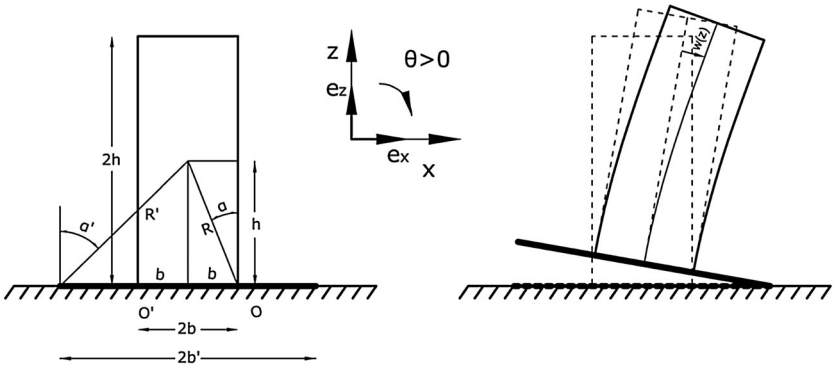

Figure 14. A flexible column monolithically connected to an extended rigid base that is allowed to uplift.

DOI: 10.1002/eqe

resulting in $r' \approx r = \left(1 - \frac{3}{2}\sin^2\alpha\right)^2$ for small α and α'. Hence, for small α' rigid columns with the same footing width $2b'$ and the same column height $2h$ behave identically, no matter what their actual width $2b$ is.

This approach is extended from rigid to flexible columns using Equation (20). The overturning stability of a flexible column connected to rigid base is given by

$$\theta(t) = \varphi\left(\frac{a_p}{g\tan\alpha}, \frac{\omega_p}{p}, \alpha, \zeta, \frac{E}{\rho g R}, \alpha'\right) \tag{28}$$

The dynamic response of this system to a ground motion excitation is modeled in OpenSees using the SM with added rotational masses. The elastic nonlinear spring at the base of the column has a yield moment equal to $mgR'\sin\alpha'$. The total added rotational mass that is distributed to the column nodes of the model is $\Delta I = mR^2\left(\frac{1}{3} + \frac{\cos\alpha}{\cos\alpha} - \frac{4}{3}\cos^2\alpha\right)$. The viscous damping coefficient of the rotational spring was computed using Equation (17), while the damping ratio of the flexible column ζ was set to 0.01. Slenderness $\tan\alpha' = 0.3$ is an upper bound to α' since for larger values the energy dissipated at every impact becomes too large to be described by the proposed SM viscous damping model.

The overturning spectra (contours of normalized maximum rotation θ/α) excited by a symmetric Ricker pulse of amplitude a_p and cyclic frequency ω_p computed using the SM with the added rotational masses are plotted in Figure 15 for a quasi-rigid column and four different flexible rocking column heights with two different slenderness ratios. The flexible rocking bodies are assumed to be of concrete ($E = 30GPa$ and $\rho = 2.5\mathrm{Mg}/m^3$). The bold lines, defining the uplift initiation, rocking and overturning regions in the spectra plotted in Figure 15, are re-plotted in Figure 16 (top). Despite the change of the aspect ratio of the rocking flexible column through the use of an extended rigid base, the effect of column flexibility is negligible for $\tan\alpha > 0.2$. For columns with $\tan\alpha = 0.1$, the flexibility of the column influences the response only in the case of columns taller than 50m and for ω_p/p smaller than 4. For this size of columns, these values of ω_p/p

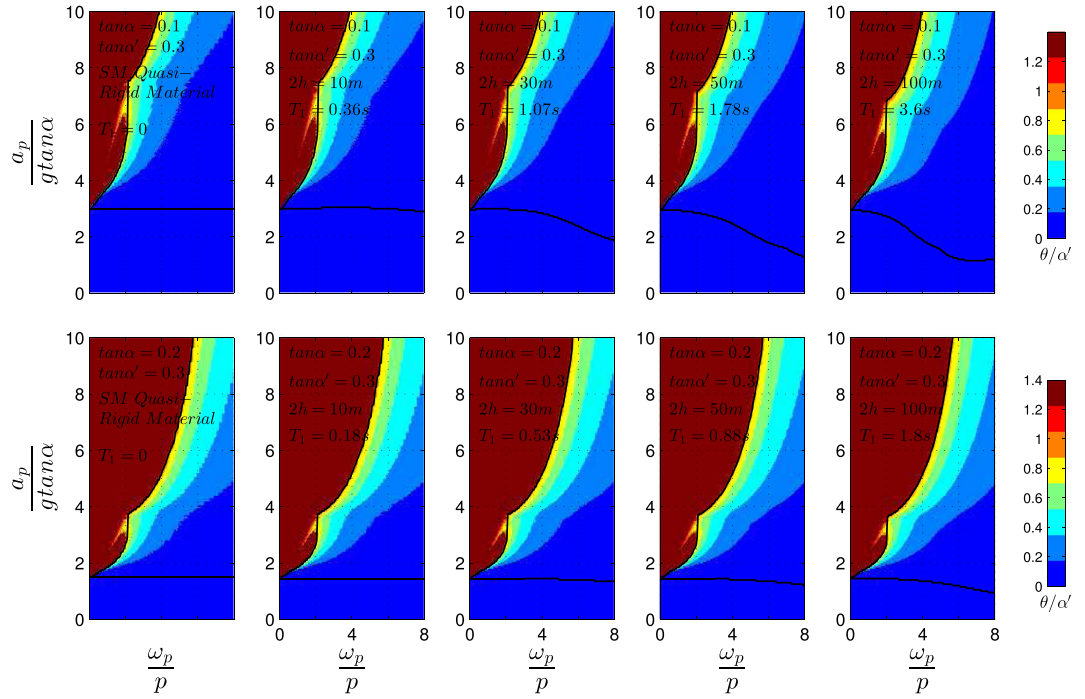

Figure 15. Contour plots of the normalized rotation, θ/α, of concrete (E = 30GPa, ρ = 2.5Mg/m^3) columns with height 2h and slenderness α connected to a rigid base with $\tan\alpha' = 0.3$ subjected to a symmetric Ricker acceleration pulse with amplitude a_p and cyclic frequency ω_p. The bold lines define the margin between uplift and no-uplift regions as well as the minimum acceleration to cause overturn.

DOI: 10.1002/eqe

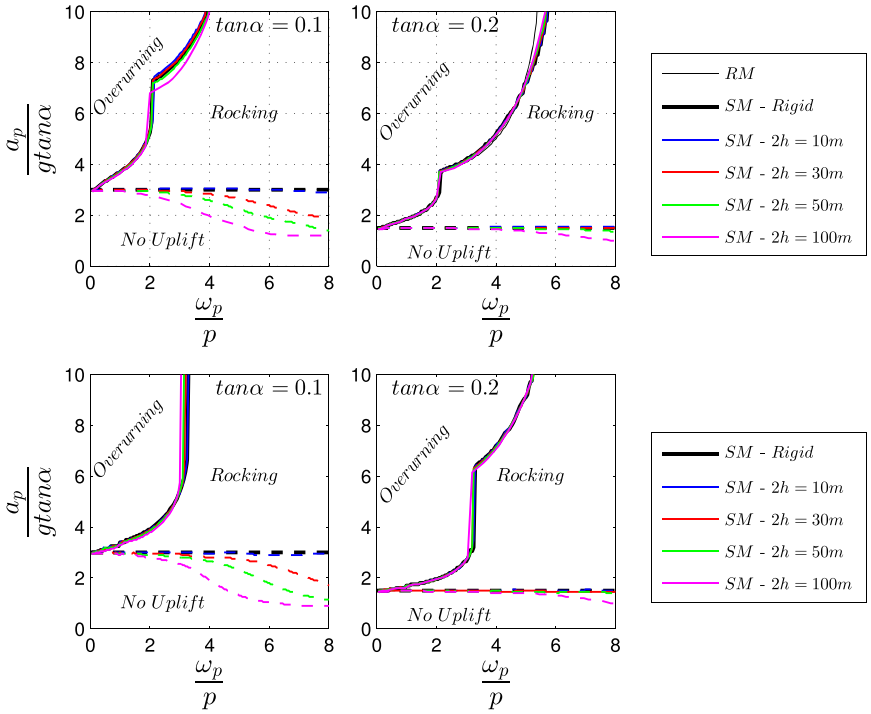

Figure 16. Minimum uplift and overturning acceleration spectra of concrete (E = 30GPa, ρ = 2.5Mg/m^3) columns with height 2h and slenderness α connected to a rigid base with tan $\alpha' = 0.3$ subjected to a symmetric (top) or antisymmetric (bottom) Ricker acceleration pulse with amplitude a_p and cyclic frequency ω_p.

correspond to unrealistic pulses with pulse periods longer than 3 seconds. Figure 16 (bottom) shows that the same results hold for an antisymmetric ($f(t) = -f(-t)$) Ricker pulse excitation given by

$$\ddot{u}_g(t) = \frac{a_p}{\beta}\left(\frac{\omega_p{}^2 t^2}{3} - 3\right)\frac{\omega_p t}{\sqrt{3}} e^{-\frac{1}{2}\frac{\omega_p{}^2 t^2}{3}} \tag{29}$$

in which β is a factor equal to 1.38 that forces the above function to have a maximum equal to a_p. For hollow cross sections, which are stiffer and lighter, the effects of flexibility are expected to be even less. Based on these findings, it is recommended to use the RM to describe the rocking motion of flexible, solid or hollow, rectangular cross section columns with a slenderness as low as $\tan\alpha = 0.1$ and a height as large as 100m, connected to a base up to 3 times larger than their width subjected to pulse-like ground motions.

6. RESPONSE OF A FLEXIBLE ROCKING CHIMNEY EXCITED BY EARTHQUAKE GROUND MOTIONS

Rocking structures date back to ancient times. However, there is no historical evidence that ancient engineers actually designed rocking structures with their seismic rocking behavior in mind. To the best of the authors' knowledge, the first engineered use of rocking as a seismic response modification mechanism was for a bridge over the Rangitikei River in New Zealand in 1981 (Beck and Skinner [17], Ma and Khan [35]) and for a rocking chimney at the Christchurch Airport (Sharpe and Skinner [36]). The 33m tall Christchurch airport chimney has a cruciform base cross section with a 7.5m × 7.5m footprint. The chimney is designed so that it can rock during large earthquakes. It is equipped with a system that allows for the rocking motion, while preventing the chimney from walking off the foundation. Additional energy dissipation is provided by steel hysteretic dampers installed at the chimney base. Sharpe and Skinner [36] mention that the chimney's "freedom to rock

DOI: 10.1002/eqe

gives it the ability to withstand very large earthquakes without requiring the substantial repairs that most reinforced concrete structures would need".

Since it has a cruciform cross section, the rigid RM is not strictly applicable because cruciform cross sections are more flexible than solid or hollow cross sections with the same area. Hence, the flexibility of the chimney may significantly affect its response. Thus, the chimney was modeled using the SM with added rotational masses. For simplicity, the chimney was modeled as elastic and made of concrete ($E = 30GPa$ and $\rho = 2.5\mathrm{M}g/m^3$) with a constant cross section ($I_{xx} = 2.99m^4$ and $A = 1.74m^2$). The damping ratio of the chimney above the base was set to 0.01. The stiffness and damping of the SM were modeled as proposed above. Two different base models were created: one with the original foundation width of 7.5m, giving the structure a slenderness $\tan\alpha = 7.5/32.65 = 0.23$ and making it capable of uplifting and rocking, and the other with a foundation wide enough such that the chimney model does not uplift, so the column of the SM behaves as if it were fixed at its base.

The response time histories of the three Christchurch Airport chimney models excited by the NS component of the El Centro 18.5.1940 ground motion, which was used in the original paper by Sharpe and Skinner [36], are plotted in Figure 17. The rocking chimney develops a maximum base moment M_{base} of 7327 kNm while the fixed-base one develops a significantly larger 33200 kNm moment. Hence, the chimney and the foundation can be designed using less than a quarter of the

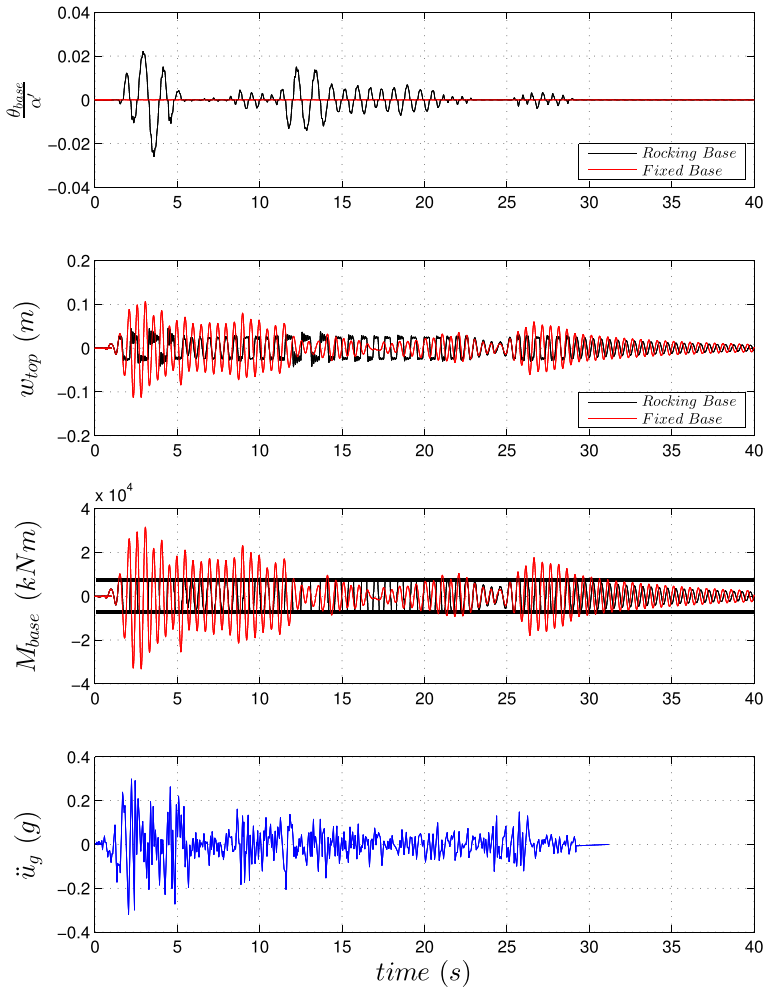

Figure 17. Response time histories of the Christchurch Airport chimney based on the original foundation (rocking) and on a foundation large enough not to uplift (fixed-base). First row: normalized base rotation; second row: top displacement due to bending; third row: bending moment at the base; fourth row: ground acceleration (El Centro 18.5.1940 ground motion, NS Component).

DOI: 10.1002/eqe

moment that would develop if the chimney was designed not to uplift. The maximum rotation of the chimney computed using the SM model is as small as 0.027 a' (i.e., less than 4% of the rotation that would cause overturning). Figure 17 (top) also compares the rotation time histories obtained using the SM and the RM uplifting models and shows they are quite different because the chimney is flexible. Coincidently, the maximum rotations computed using the SM and the RM uplifting models are virtually the same, even though the RM is not strictly applicable.

7. SYNOPSIS AND CONCLUSIONS

A model for analysis of the dynamic response of flexible rocking bodies was proposed. This model does not explicitly model rocking impact. Instead, it utilizes a nonlinear elastic rotational spring and a linear viscous rotational damper, located at the rocking body centerline, to model the rocking interface. The rotational spring exhibits a nonlinear-elastic behavior and the damper is calibrated to dissipate the same amount of energy as is dissipated through impact in a single rocking cycle. The rocking body is modeled as a multi-node linear elastic beam-column, with rotational inertia added to the nodes to correct for the translation of the center of rotation from the edges to the centerline of the rocking body. The principal advantages of this model are that it is computationally efficient and it can be implemented in conventional finite element analysis software with large deformation and nonlinear-elastic spring element capabilities. The model was first verified against the numerical solution of Housner's equation for a rocking rigid block with excellent results. Then, the model was implemented in OpenSees and used to study the effect of flexibility on the rocking response of solitary columns with solid rectangular cross sections to analytical pulse excitations. The effect of column flexibility is negligible for solitary columns up to 30m tall. For taller columns (and for realistically long pulses) flexibility increases the overturning acceleration. The latter is a result of the transformation of the rotational kinetic energy to bending vibrations at each rocking impact. The model was used to examine the seismic performance of an existing rocking chimney. It was found that the chimney exhibits remarkable stability and the expected control of base moment demand under earthquake excitation. Therefore, the non-linear elastic viscously damped zero-length spring model is recommended for dynamic response analysis of rocking elastic bodies whose response does not depend significantly on the change of centerline distance between the rocking edges subjected to pulse-like ground motions.

REFERENCES

1. Milne J. Seismic experiments. *Transactions of the Seismological Society of Japan* 1885; **8**:1–82.
2. Housner GW. The behaviour of inverted pendulum structures during earthquakes. *Bulletin of the Seismological Society of America* 1963; **53**(2):404–417.
3. Zhang J, Makris N. Rocking response of free-standing blocks under cycloidal pulses. *Journal of Engineering Mechanics, ASCE* 2001; **127**(5):473–483.
4. Makris N, Konstantinidis D. The rocking spectrum and the limitations of practical design methodologies. *Earthquake Engineering and Structural Dynamics* 2003; **32**:265–289.
5. Palermo A, Pampanin S, Carr A. Efficiency of simplified alternative modelling approaches to predict the seismic response of precast concrete hybrid systems. *fib Symposium "Keep Concrete Attractive"*, Budapest, 2005.
6. Psycharis IN. Dynamics of flexible systems with partial lift-off. *Earthquake Engineering and Structural Dynamics* 1983; **11**(4):501–521.
7. Ichinose T. Rocking motion of slender elastic body on rigid floor. *Bulletin of the New Zealand National Society for Earthquake Engineering* 1986; **19**(1):18–27.
8. Oliveto G, Caliò I, Greco A. Large displacement behaviour of a structural model with foundation uplift under impulsive and earthquake excitations. *Earthquake Engineering and Structural Dynamics* 2003; **32**:369–393.
9. Spyrakos CC, Nikolettos GS. Overturning stability criteria for flexible structures to earthquakes. *Journal of Engineering Mechanics* 2005; **131**(4):349–358.
10. Apostolou M, Gazetas G, Garini E. Seismic response of slender rigid structures with foundation uplifting. *Soil Dynamics and Earthquake Engineering* 2007; **27**(7):642–654.
11. Acikgoz S, DeJong MJ. The interaction of elasticity and rocking in flexible structures allowed to uplift. *Earthquake Engineering and Structural Dynamics* 2012. DOI: 10.1002/eqe.2181
12. Meek JW. Dynamic response of tipping core buildings. *Earthquake Engineering and Structural Dynamics* 1978; **6**(5):437–454.

13. Chopra AK, Yim SCS. Simplified earthquake analysis of structures with foundation uplift. *Journal of Structural Engineering* 1985; **111**(4):906–930.
14. Psycharis IN. Effect of base uplift on dynamic response of SDOF structures. *Journal of Structural Engineering* 1991; **117**(3):733–754.
15. Gelagoti F, Kourkoulis R, Anastasopoulos I, Gazetas G. Rocking isolation of low-rise frame structures founded on isolated footings. *Earthquake Engineering and Structural Dynamics* 2012; **41**:1177–1197.
16. Makris N, Vassiliou MF. Planar rocking response and stability analysis of an array of free-standing columns capped with a freely supported rigid beam. *Earthquake Engineering and Structural Dynamics* 2013; **42**:431–449.
17. Beck JL, Skinner RI. The seismic response of a reinforced concrete bridge pier designed to step. *Earthquake Engineering and Structural Dynamics* 1973; **2**: 343–358.
18. Konstantinidis D, Makris N. Seismic response analysis of multidrum classical columns. *Earthquake Engineering and Structural Dynamics* 2005; **34**:1243–1270.
19. Yim CS, Chopra AK, Penzien J. Rocking response of rigid blocks to earthquakes. *Earthquake Engineering and Structural Dynamics* 1980; **8**(6):565–587.
20. Makris N, Roussos Y. Rocking response of rigid blocks under near-source ground motions. *Geotechnique* 2000; **50**(3):243–262.
21. Dimitrakopoulos EG, DeJong MJ. Overturning of Retrofitted Rocking Structures under Pulse-Type Excitations. *Journal of Engineering Mechanics* 2012; **138**(8):963–972.
22. MATLAB Version 2011b. *The Language of Technical Computing*. The Mathworks, Inc.: Natick, MA, 1999.
23. OpenSEES (Open System for Earthquake Engineering Simulation). opensees.berkeley.edu
24. Barthes C, Hube M, Stojadinovic B. Dynamics of a Post-Tensioned Rocking Block. *Proceedings of the 9th US National and 10th Canadian Conference on Earthquake Engineering*, Toronto, Canada, July 25–29, 2010.
25. Ricker N. Further developments in the wavelet theory of seismogram structure. *Bulletin of the Seismological Society of America* 1943; **33**:197–228.
26. Harden CW, Hutchinson TC. Beam-on-nonlinear-Winkler-foundation modeling of shallow, rocking-dominated footings. *Earthquake Spectra* 2009; **25**(2):277–300.
27. Marriott D, Pampanin S, Palermo A, Bull D. Dynamic testing of precast, post-tensioned rocking wall systems with alternative dissipating solutions. *Bulletin of NZSEE* 2008; **41**(2):90–103.
28. Wiebe L, Christopoulos C, Tremblay R, Leclerc M. Modelling inherent damping for rocking systems: results of large-scale shake table testing. *Proceedings of the 15th World Conference on Earthquake Engineering*, Lisbon, Portugal, 2012.
29. Barenblatt GI. *Scaling, self-similarity, and intermediate asymptotics*. Cambridge University Press: Cambridge, U.K., 1996.
30. ElGawady MA, Ma Q, Butterworth JW, Ingham J. Effects of interface material on the performance of free rocking blocks. *Earthquake Engineering and Structural Dynamics* 2011; **40**:375–392.
31. Roh H, Reinhorn A. Modeling and seismic response of structures with concrete rocking columns and viscous dampers. *Engineering Structures* 2010; **32**(8):2096–2107.
32. Pecker A, Pender MJ. Earthquake resistant design of foundations: new construction. *Invited paper. GeoEng Conference*, Melbourne 2000; **1**:313–332.
33. Kawashima K, Nagai T, Sakellaraki D. Rocking seismic isolation of bridges supported by spread foundations. *Proceedings of the of 2nd Japan-Greece Workshop on Seismic Design, Observation, and Retrofit of Foundations*, vol. **1**, Tokyo, Japan, 2007; 254–265.
34. Anastasopoulos I, Gazetas G, Loli M, Apostolou M, Gerolymos N. Soil failure can be used for earthquake protection of structures. *Bulletin of Earthquake Engineering* 2010; **8**:309–326.
35. Ma QT, Khan MH. Free vibration tests of a scale model of the South Rangitikei Railway Bridge. *Proceedings of the New Zealand Society for Earthquake Engineering Annual Conference, Engineering an Earthquake Resilient NZ*, 2008.
36. Sharpe RD, Skinner RI. The seismic design of an industrial chimney with rocking base. *Bulletin of the New Zealand National Society for Earthquake Engineering* 1983; **16**(2):98–106.

DOI: 10.1002/eqe